Supporting information

A dual-mode MOF sensor for Al^{3+} detection based on red-shift ratiometric fluorescence and portable hydrogel-smartphone analysis

Yun Cao[§], Mengting Zhao[§], Yuxuan Zhang, Chunyin Ye, Junuo Zhang, Yan Wang*

Anhui Provincial Key Laboratory of Advanced Catalysis and Energy Materials, Anhui Key Laboratory of Optoelectronic Magnetic Functional Complex and Nano Complex, School of Chemistry and Chemical Engineering, Anqing Normal University, Anqing 246011, PR China

[§] The authors contributed equally to this work.

* Correspondence: wangyan@aqnu.edu.cn

Experimental section

Materials

All reagents, except for ligand L1 which was synthesized according to literature procedures [1], were directly purchased and used without additional purification. Cadmium nitrate tetrahydrate ($Cd(NO_3)_3·4H_2O$, ≥99.0%), 4,4'-biphenyldicarboxylic acid (H_2bpdc, ≥97.0%), Sulfamethazine (SMZ, ≥99.0%), Azithromycin (AZM, ≥98.0%), Chloramphenicol (CAP, ≥98.0%), Kanamycin sulfate (KAM, ≥94.0%), Roxithromycin (RXM, ≥98.0%), Sulfadiazine (SDZ, ≥98.0%), Penicillin (PNC, ≥96.0%), aluminum chloride hexahydrate ($AlCl_3·6H_2O$, ≥99.99%), iron(III) chloride ($FeCl_3$, ≥98.0%), barium chloride dihydrate ($BaCl_2·2H_2O$, ≥99.0%), calcium chloride

anhydrous ($CaCl_2$, ≥96.0%), cobalt(II) chloride hexahydrate ($CoCl_2·6H_2O$, ≥99.99%), cadmium chloride hemipentahydrate ($CdCl_2·2.5H_2O$, ≥98.0%), strontium chloride hexahydrate ($SrCl_2·6H_2O$, ≥99.99%), zinc chloride ($ZnCl_2$, ≥98.0%), nickel(II) chloride hexahydrate (NiCl2·6H2O, ≥99.0%), manganese(II) chloride tetrahydrate (MnCl2·4H2O, ≥99.99%), magnesium chloride hexahydrate (MgCl2·6H2O, ≥98.0%), potassium chloride (KCl, ≥99.5%), sodium chloride (NaCl, ≥99.9%), sodium fluoride (NaF, ≥98.0%), sodium bromide (NaBr, ≥99.0%), sodium bicarbonate ($NaHCO_3$, ≥99.5%), sodium carbonate (Na_2CO_3, ≥99.8%), sodium acetate (CH_3COONa, ≥99.0%), sodium sulfate (Na_2SO_4, ≥99.0%), sodium thiosulfate ($Na_2S_2O_3$, ≥99.0%), sodium nitrate ($NaNO_3$, ≥99.0%), sodium thiocyanate (NaSCN, ≥98.0%), sodium dihydrogen phosphate (NaH_2PO_4, ≥99.0%), disodium hydrogen phosphate (Na_2HPO_4, ≥99.0%), trisodium phosphate (Na_3PO_4, ≥98.0%). All reagents were purchased from Aladdin Reagent (Aladdin) or Sinopharm Chemical Reagent Co., Ltd. (Sinopharm). All aqueous solutions used in the experiments were prepared using deionized water.

Apparatus

Elemental composition analysis was conducted using a Vario EL-III elemental analyzer manufactured by Elementar (Germany) to determine the contents of C, H, and N elements in the sample. Crystal structure characterization was accomplished through powder X-ray diffraction (PXRD) technology. The experiment was carried out at room temperature using a Rigaku D/max-RA diffractometer, with Cu-Kα radiation (λ = 1.542 Å) and a graphite monochromator for collecting diffraction data. Fourier transform infrared spectroscopy (FT-IR) testing was performed on a Nicolet AVATAR-

350 spectrometer using the KBr pellet method, with a testing range of 500-4000 cm^{-1}. Thermogravimetric analysis (TGA) was conducted using a NETZSCH STA-409PC thermal analyzer in a nitrogen atmosphere, with a heating rate of 10°C/min from room temperature to 800°C to investigate the thermal decomposition behavior of the material.

For optical property characterization, solid-state fluorescence spectra were measured using a Hitachi F-74500 fluorescence spectrophotometer, and fluorescence decay curves were obtained using an Edinburgh FS5 fluorescence spectrometer. PL quantum yields (PLQYs) were measured on a Hamamatsu (C11347) absolute PLQY spectrometer. Ultraviolet-visible absorption spectra were determined using a Shimadzu UV-2400 spectrophotometer. Additionally, Scanning Electron Microscope (SEM) (Hitachi SU8600, Japan) Used to characterize the morphology of the material and energy dispersive *X-ray* spectroscopy (EDS) using the same SEM equipment Chemical mapping. *X-ray* photoelectron spectroscopy (XPS) was acquired on an AXIS Ultra DLD spectrometer.

Single-crystal X-ray diffraction analysis

X-ray diffraction data were collected at room temperature using a Bruker SMART APEX CCD diffractometer (with Mo-Kα radiation, λ = 0.71073 Å). The crystal was kept at 301.00 K during data collection. Using Olex2,[2] the structure was solved with the olex2.solve [3] structure solution program using Charge Flipping and refined with the SHELXL [4] refinement package using Least Squares minimization. During the structure refinement, all non-hydrogen atoms were treated with anisotropic displacement parameters, and the hydrogen atoms of the organic ligands were

positioned geometrically. The principal crystallographic parameters for complex **1** are summarized in **Table S1**, while the characteristic bond lengths and bond angles are presented in **Tables S2**. The crystal structure data have been deposited with the Cambridge Crystallographic Data Centre (CCDC number: 2456368).

Fluorescence detection of Fe^{3+} and Al^{3+}

Detection of Fe^{3}: Complex **1** was dispersed in deionized water after grinding and subjected to 30 minutes of ultrasonic treatment to obtain a uniform dispersion system with a concentration of 0.5 mg/mL. Two milliliters of this dispersion were placed in a quartz cuvette, and changes in fluorescence emission intensity at 347 nm were monitored under an excitation wavelength of 315 nm, yielding a Stokes shift of 32 cm^{-1} (**Figure. S1a**). To evaluate detection sensitivity, standard solutions of Fe^{3+} at different concentration gradients were sequentially added to the MOF dispersion system. Thorough mixing was performed after each addition, followed by acquisition of the corresponding fluorescence spectra. Prior to analyzing target ions, multiple potential interfering species were pre-introduced into the complex **1** dispersion to systematically assess the method's selectivity and interference resistance.

Detection of Al^{3+}: Complex **1** was prepared as a 0.5 mg/mL aqueous dispersion using the same method. Two milliliters of this dispersion were placed in a quartz cuvette, and the fluorescence emission intensity at 400 nm was recorded under excitation at 315 nm, yielding a Stokes shift of 85 cm^{-1} (**Figure. S1b**). After reacting the complex **1** dispersion with a series of Al^{3+} solutions at varying concentrations, the fluorescence intensity ratio at 347 nm to 400 nm (I_{347}/I_{400}) was measured upon

excitation at 315 nm. This ratio exhibited a good linear dependence on Al^{3+} concentration, enabling the construction of a quantitative calibration curve. Prior to Al^{3+} detection, the specificity and interference tolerance of this method were comprehensively evaluated by introducing various competitive substances, including cations, anions, and antibiotics, into the system.

Construction of a smartphone-based gel matrix visual sensing platform for Al^{3+} detection

Complex **1** was loaded onto agarose hydrogel via solution polymerization. Specifically, 150 mg of agarose hydrogel and 10 mg of complex **1** powder were dispersed in 10 mL of ultrapure water, followed by heating to 90 °C with continuous stirring until a transparent and viscous liquid was formed.[5] The prepared agarose viscous liquid was then added to the caps of centrifuge tubes to form hydrogels. At room temperature, different concentrations of Al^{3+} solutions were added to the hydrogel system, and the centrifuge tubes were inverted. Meanwhile, mixtures of Al^{3+} standard solutions with different concentrations and complex **1** were placed in centrifuge tubes under dark conditions. All systems were subjected to fluorescence color development under excitation with a 254 nm UV light source. All fluorescence images for RGB analysis were captured using a dark-box ultraviolet lamp setup to ensure consistent illumination conditions. The samples were placed in a fixed position within the dark box, and the ultraviolet lamp was operated at a constant intensity. Fluorescence images of the systems were captured using a smartphone. The red, green, and blue (RGB) chromaticity parameters were extracted with a professional color analysis software

(Color Recognizer, China). By analyzing the correlation between the changes in RGB values and Al^{3+} concentrations, the visual assessment of Al^{3+} was achieved.

Determination of Al^{3+} in real water samples.

The actual water samples used in the experiments included lake and tap water taken from the Longshan Campus of Anqing Normal University, as well as water samples of the Yangtze River collected from Anqing City. All water samples were triple-filtered through a 0.22 μm mixed cellulose ester microporous filter membrane to remove insoluble impurities, and were subsequently used to prepare test solutions containing Al^{3+}. The subsequent experimental manipulations were consistent with the fluorescence experiments.

Powder X-ray Diffraction (PXRD) of Zn-based complex in comparison with the Cd-MOF counterparts

In this study, attempts were also made to assemble functional materials using zinc salts, which are less toxic and belong to the same group as cadmium, under similar synthesis conditions. However, no suitable single crystals were obtained for structural analysis. Under these circumstances, powder X-ray diffraction (PXRD) was employed for a tentative characterization of the zinc-based structure. The obtained PXRD pattern of the zinc complex exhibited significant differences from that of its cadmium counterpart, as illustrated in the Figure S14. The considerable discrepancies in the diffraction peaks suggest distinct differences in the microscopic crystal structures between the two compounds, which may also account for the unsuccessful acquisition of single-crystal samples of the zinc complex under similar hydrothermal synthesis

conditions. Thus, in the absence of crystal structure analysis, no further investigation was conducted into the recognition properties of the zinc complex.

Table S1. Crystallography parameters of complex **1**

Complex	**1**
Empirical formula	$C_{33}H_{42}CdN_4O_9$
Formula weight	751.10
Temperature/K	301.00
Crystal System	triclinic
Space group	$P\bar{1}$
a/Å	11.9413(5)
b/Å	12.4268(5)
c/Å	12.4788(4)
α/°	76.9542(10)
β/°	88.8155(11)
γ/°	71.1537(11)
Volume/Å^3	1704.51(11)
Z	2
μ, mm^{-1}	0.699
ρ_{calc} g cm^{-3}	1.463
$F_{(000)}$	776.0
θ/°	2.08-24.996
Measured refls.	41214
Independent refls.	5931
R_{int}	0.1565

R_1/wR_2 (Final)	0.0395/ 0.0955
R_1/wR_2 (all data)	0.0454/ 0.0987
Δρmax/Δρmin, e/Å^{-3}	0.65/-0.40

$R_1 = \Sigma||F_o| - |F_c||/\Sigma|F_o|$. $wR = |\Sigma w(|F_o|^2 - |F_c|^2)^2|/\Sigma|w(F_o)^2|^{1/2}$.

Table S2. Selected bond lengths (Å) and bond angles (°) of complex **1**

Parameter	Value	Parameter	Value
Complex **1**			
Cd1-O1	2.365(3)	Cd1-N1	2.297(3)
Cd1-O2	2.355(2)	Cd1-N3$^{\#1}$	2.229(2)
Cd1-O4	2.246(2)		
O2-Cd1-O1	54.66(9)	N1-Cd1-O2	109.67(10)
O4-Cd1-O1	88.62(10)	N3$^{\#1}$-Cd1-O1	148.18(10)
O4-Cd1-O2	142.24(10)	N3$^{\#1}$-Cd1-O2	97.96(9)
O4-Cd1-N1	88.46(10)	N3$^{\#1}$-Cd1-O4	113.48(9)
N1-Cd1-O1	108.41(11)	N3$^{\#1}$-Cd1-N1	95.35(10)
Symmetry code for **1**：#1 x, y, -1+z			

Table S3. Hydrogen bond length (Å) and bond angle (°) of complex **1**.

D-H···A	D-H	H···A	D···A	D-H···A
O1W-H1WA···O3W$^{\#1}$	0.85	2.16	3.001(9)	173
O1W-H1WB···O5W$^{\#1}$	0.85	1.95	2.797(6)	173

O2W-H2WA···O4$^{\#2}$	0.85	2.12	2.967(5)	172
O2W-H2WB···O4W$^{\#1}$	0.85	2.12	2.964(8)	172
O3W-H3WA···O1$^{\#2}$	0.85	2.14	2.967(7)	163
O3W-H3WB···O2W$^{\#2}$	0.85	2.20	3.021(10)	163
O4W-H4WA···O3W$^{\#2}$	0.85	2.06	2.910(9)	174
O4W-H4WB···O5W$^{\#2}$	0.85	1.99	2.834(7)	174
O5W-H5WA···O1$^{\#1}$	0.96	2.07	2.969(5)	155
O5W-H5WB···O3$^{\#3}$	0.96	1.96	2.906(4)	168

Symmetry codes: #1 1-x, 1-y, 1-z; #2 x, y, z; #3 x, y, 1+z.

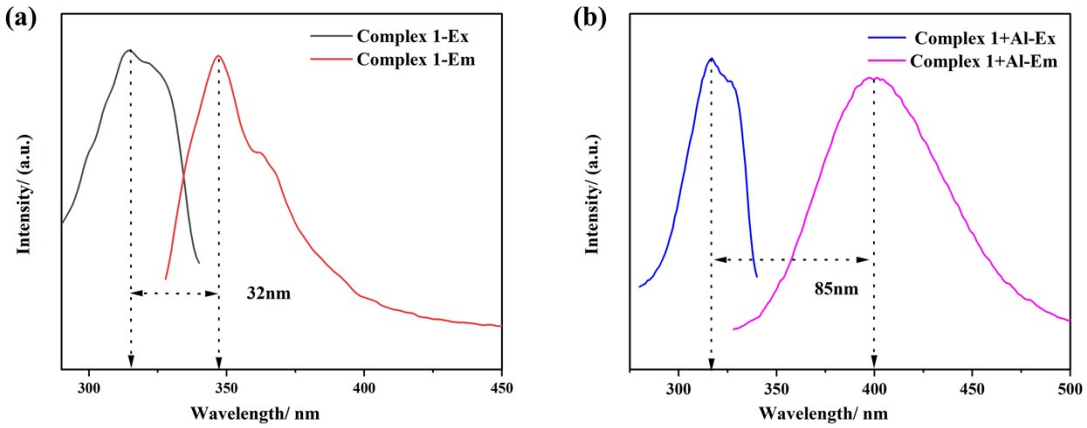

Figure S1. (a) Excitation and emission spectra of complex **1** in aqueous solution; (b) Excitation and emission spectra of complex **1** in Al^{3+} solution.

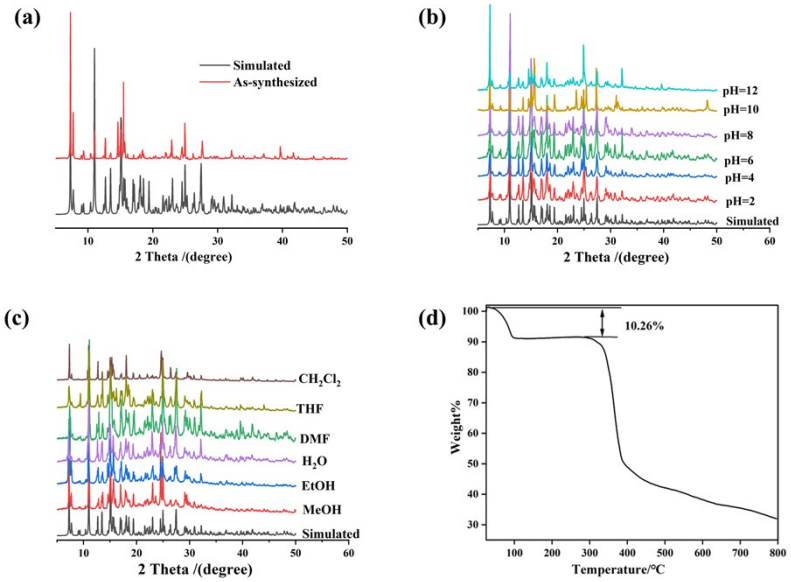

Figure S2. (a) PXRD patterns of simulation and as-synthesized; (b) PXRD patterns of complex **1** soaked in aqueous solutions at pH 2-12; (c) PXRD patterns of complex **1** soaked in common organic solvents; (d) Thermogravimetric diagram of complex **1.**

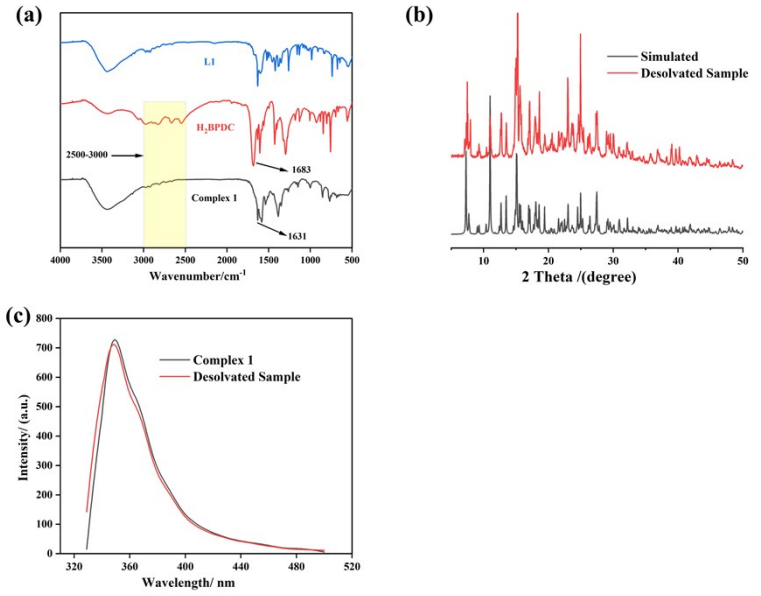

Figure S3. (a) FT-IR spectra of complex **1**, ligand L1 and H_2bpdc; (b) PXRD patterns of simulation and dehydrated sample; (c) Solid-state fluorescence emission spectra before and after dehydration.

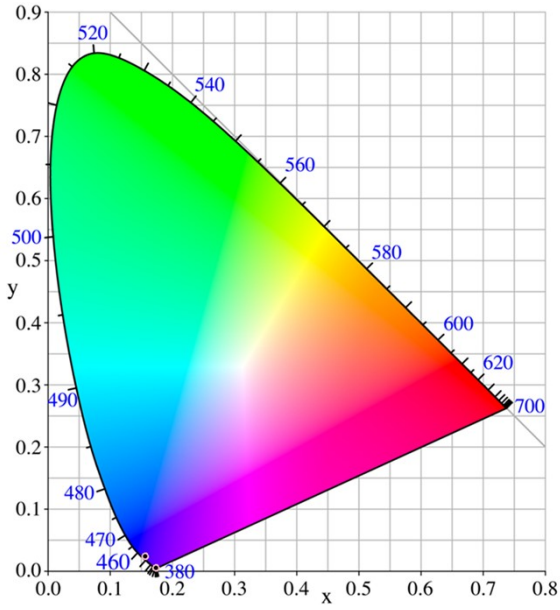

Figure S4. Comparison of CIE colorimetric coordinates of complex **1** in aqueous and Al^{3+} solutions.

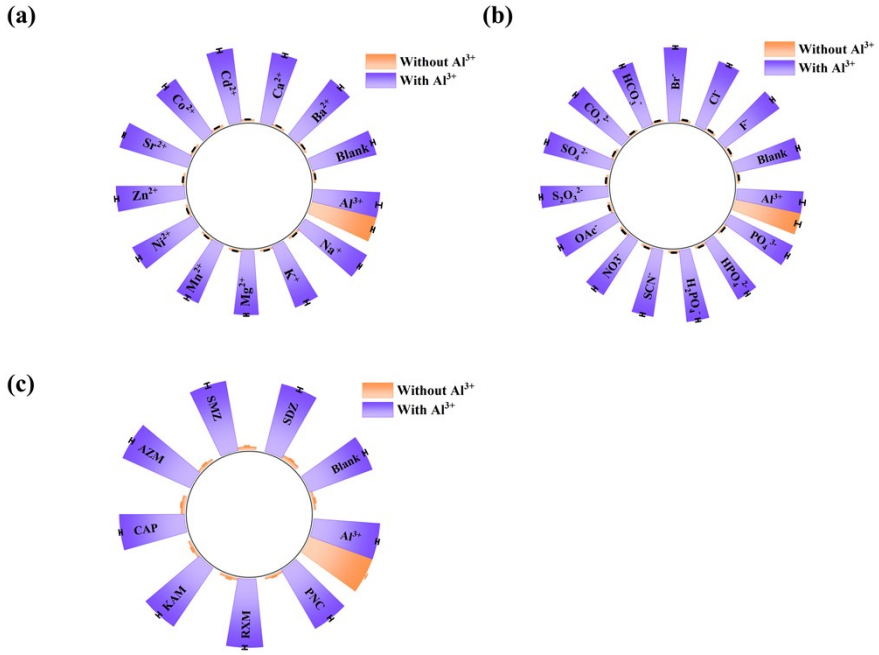

Figure S5. Radar plots for evaluating the anti-interference performance of complex **1**

in Al^{3+} detection based on the fluorescence intensity ratio (I_{400}/I_{347}): (a) Anti-interference tests with anions; (b) Anti-interference tests with cations; (c) Anti-interference tests with antibiotics.

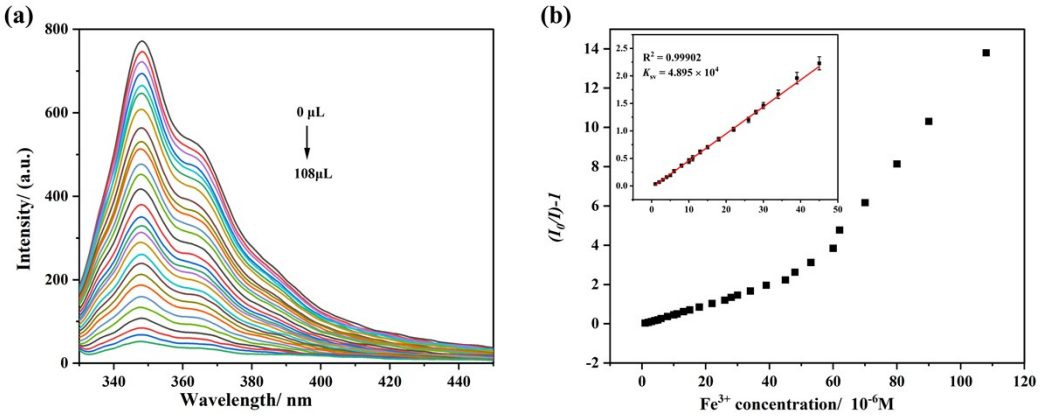

Figure S6. (a) Changes in fluorescence emission spectra of complex **1** in the presence of different Fe^{3+} concentrations; (b) Linear relationships between fluorescence intensity and Fe^{3+} concentrations.

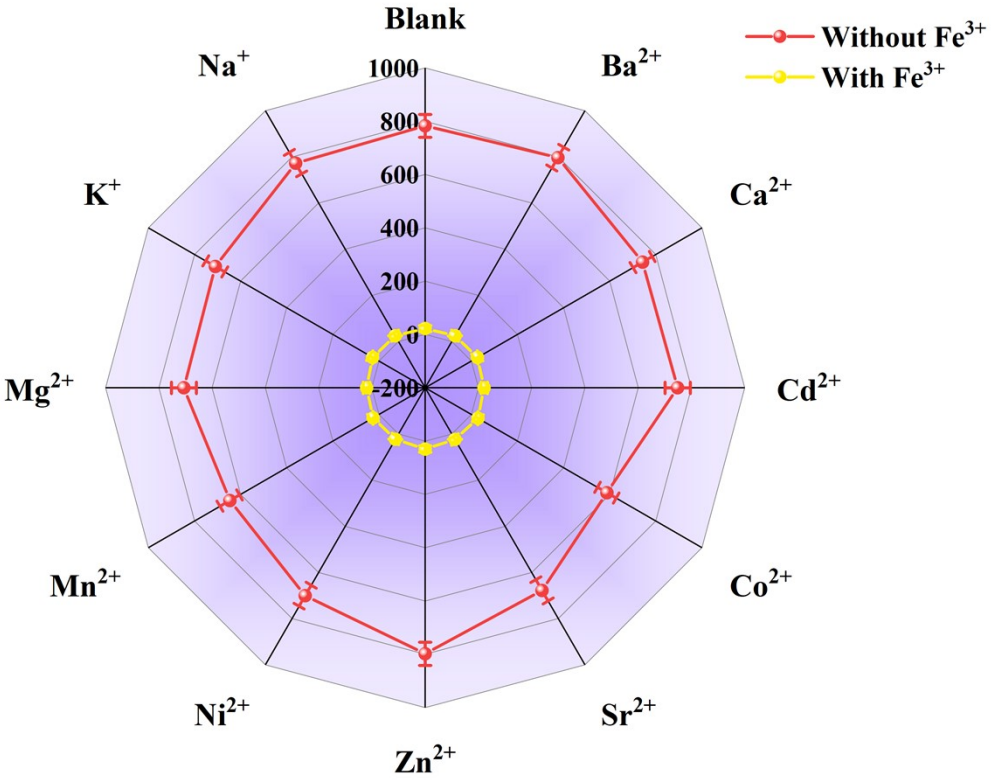

Figure S7. Radar chart of interference test responses for metal ions in complex **1** with and without Fe^{3+}.

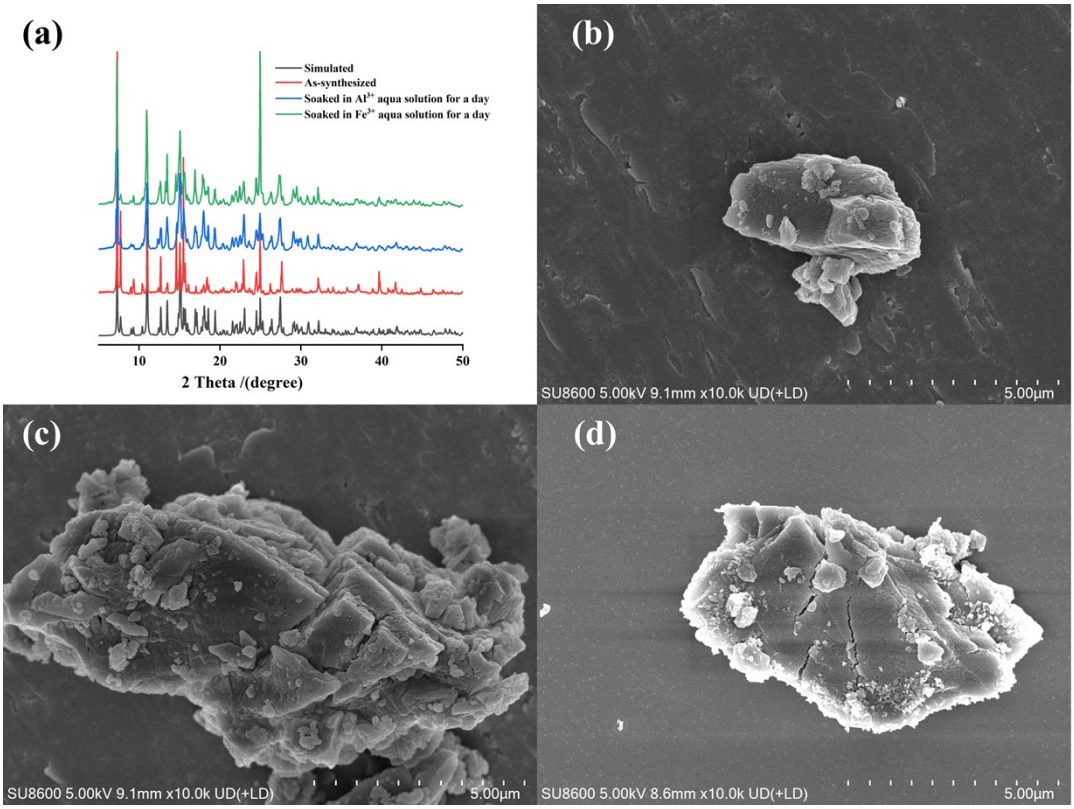

Figure S8. (a) PXRD spectra of complex **1** after immersion in aqueous solutions of Al^{3+} and Fe^{3+} ions; SEM characterization of complex **1**: (b) original sample; (c) after 24 h immersion in 0.001 M Al^{3+} solution; (d) after 24 h immersion in 0.001 M Fe^{3+} solution.

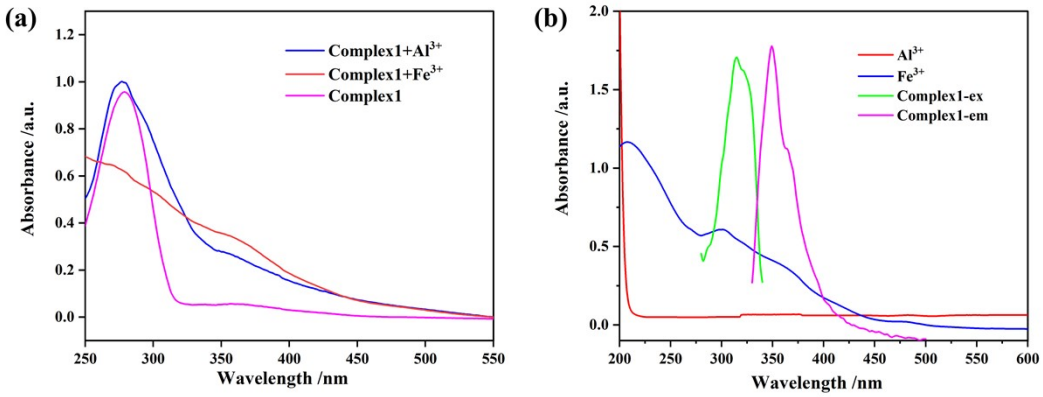

Figure S9. (a) UV-Vis absorption spectra of complex **1** in aqueous solution before and

after the addition of Al^{3+} and Fe^{3+} solutions; (c) Excitation and emission spectra of complex **1**, and UV-vis absorption spectra in Al^{3+} and Fe^{3+} solutions.

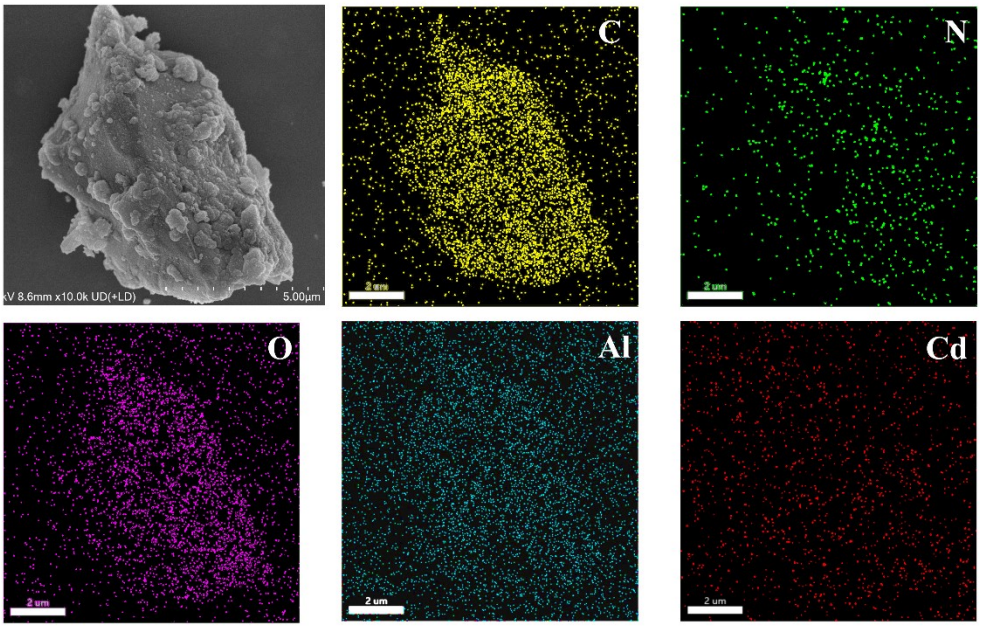

Figure S10. EDS spectra of complex **1** immersed in 0.001 M aqueous Al^{3+} ion solution for one day.

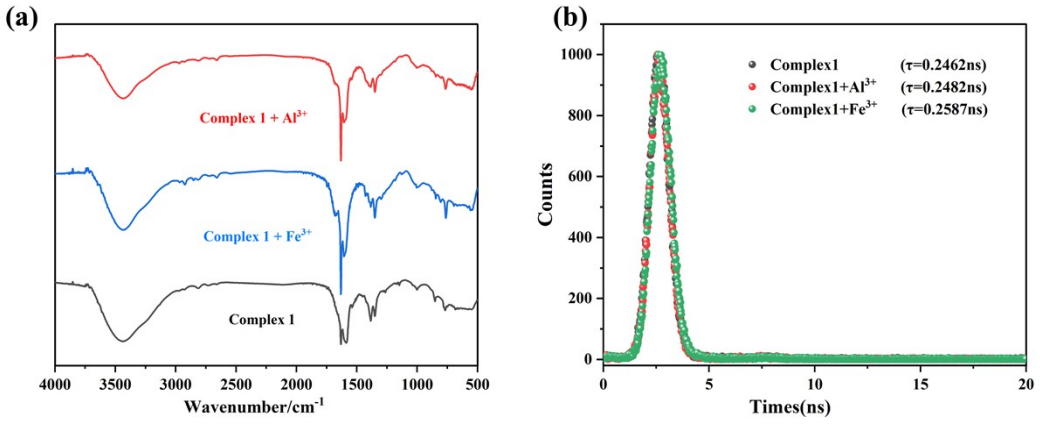

Figure S11. (a) FT-IR spectra of complex **1** before and after immersion in Al^{3+} and Fe^{3+} solutions; (b) Fluorescence lifetime decay curves of complex **1** and its fluorescence

after immersion in aqueous solutions of Al^{3+} and Fe^{3+}.

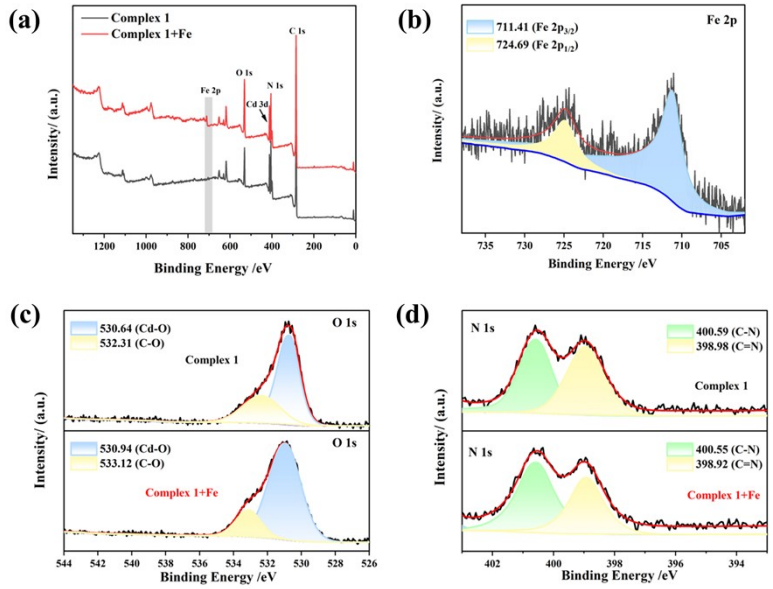

Figure S12. XPS spectra of complex **1** before and after Fe^{3+} detection; (a) Full spectrum; (b) Fe 2p spectrum; (c) O 1s spectrum; (d) N 1s spectrum.

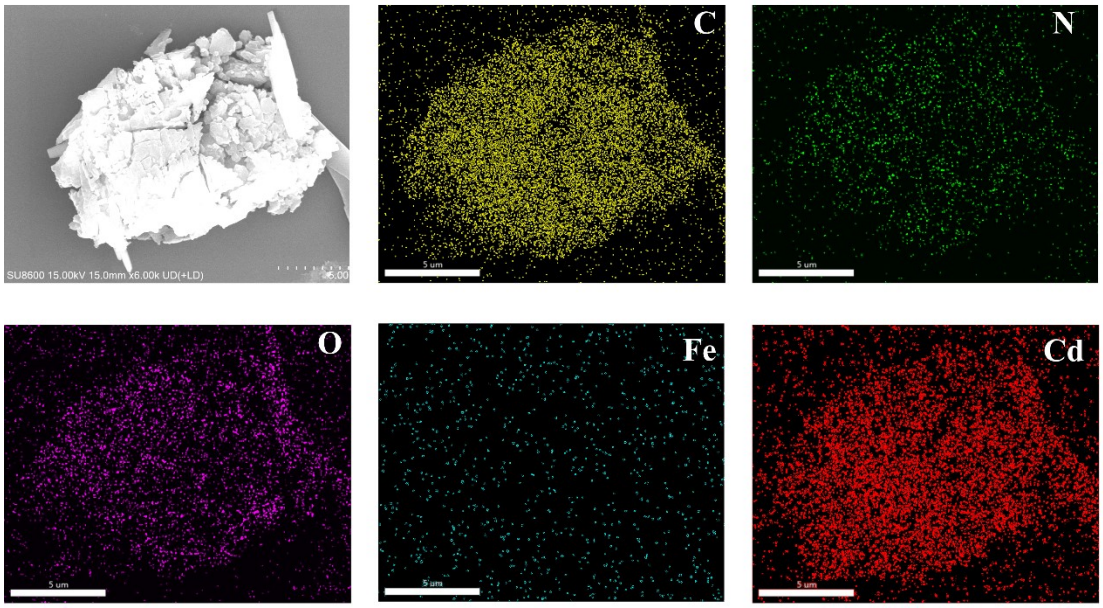

Figure S13. EDS spectra of complex **1** immersed in 0.001 M aqueous Fe^{3+} ion solution for one day.

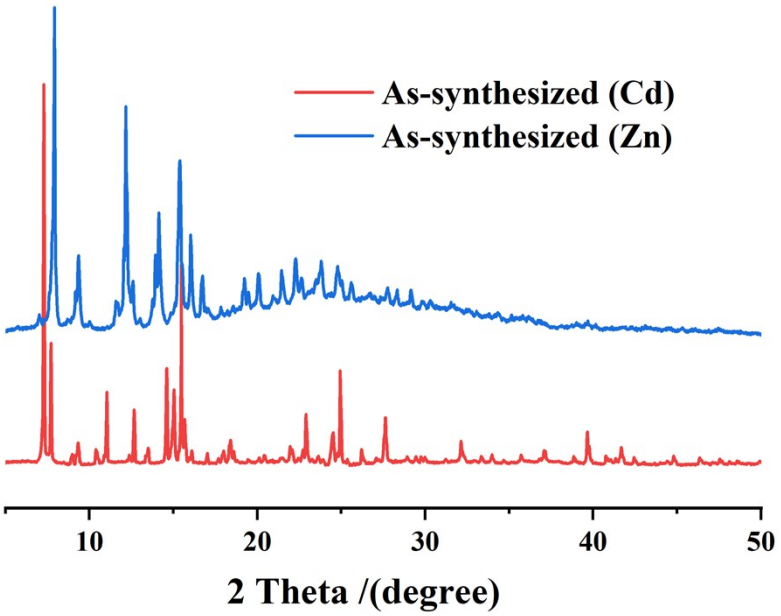

Figure S14. Comparison of the PXRD patterns between Zn-complex and Cd-complex (**1**) synthesized under same conditions.

References

1. N. N. Gao, Y. T. Ling and Y. Wang, Multi-responsive luminescent complex for Fe^{3+}, $Cr_2O_7^{2-}$ and CrO_4^{2-} species in aqueous solution based on aromatic polycarboxylic acid and imidazole-containing ligand: synthesis, crystal structure and selective detection, *J. Mol. Struct.*, 2024, **1311**, 138427.
2. O. V. Dolomanov, L. J. Bourhis, R. J. Gildea, J. A. K. Howard and H. Puschmann, OLEX2: a complete structure solution, refinement and analysis program, *J. Appl. Crystallogr.*, 2009, **42**, 339-341.
3. L. J. Bourhis, O. V. Dolomanov, R. J. Gildea, J. A. K. Howard and H. Puschmann, The anatomy of a comprehensive constrained, restrained refinement program for the modern computing environment - Olex2 dissected, *Acta Crystallographica Section A*, 2015, **71**, 59-75.
4. G. Sheldrick, Crystal structure refinement with SHELXL, *Acta Crystallographica Section C*, 2015, **71**, 3-8.
5. E. L. Wang, L. Li, J. Y. Zou, S. Y. You, R. J. Hu, L. Zhang, M. F. Wu and L. M. Dai, Regulating the Energy Level of a Ratiometric Luminescent Europium(III) Metal–Organic Framework Sensor with Smartphone Assistance for Real-Time and Visual Detection of Carcinoid Biomarker, *Inorg. Chem.*, 2025, **64**, 3930-3940.